energies

MDPI

Article

Combined Turbine and Cycle Optimization for Organic Rankine Cycle Power Systems—Part B: Application on a Case Study

Angelo La Seta [1,*], Andrea Meroni [1], Jesper Graa Andreasen [1], Leonardo Pierobon [1], Giacomo Persico [2] and Fredrik Haglind [1]

[1] Department of Mechanical Engineering, Technical University of Denmark, Nils Koppels allé, Building 403, Kongens Lyngby 2800, Denmark; andmer@mek.dtu.dk (A.M.); jgan@mek.dtu.dk (J.G.A.); lpier@mek.dtu.dk (L.P.); frh@mek.dtu.dk (F.H.)

[2] Dipartimento di Energia, Politecnico di Milano, Via Lambruschini 4, Milano 20156, Italy; giacomo.persico@polimi.it

* Correspondence: anlse@mek.dtu.dk; Tel.: +45-4525-4106

Academic Editor: Sylvain Quoilin

Received: 21 March 2016; Accepted: 18 May 2016; Published: 24 May 2016

Abstract: Organic Rankine cycle (ORC) power systems have recently emerged as promising solutions for waste heat recovery in low- and medium-size power plants. Their performance and economic feasibility strongly depend on the expander. The design process and efficiency estimation are particularly challenging due to the peculiar physical properties of the working fluid and the gas-dynamic phenomena occurring in the machine. Unlike steam Rankine and Brayton engines, organic Rankine cycle expanders combine small enthalpy drops with large expansion ratios. These features yield turbine designs with few highly-loaded stages in supersonic flow regimes. Part A of this two-part paper has presented the implementation and validation of the simulation tool TURAX, which provides the optimal preliminary design of single-stage axial-flow turbines. The authors have also presented a sensitivity analysis on the decision variables affecting the turbine design. Part B of this two-part paper presents the first application of a design method where the thermodynamic cycle optimization is combined with calculations of the maximum expander performance using the mean-line design tool described in part A. The high computational cost of the turbine optimization is tackled by building a model which gives the optimal preliminary design of an axial-flow turbine as a function of the cycle conditions. This allows for estimating the optimal expander performance for each operating condition of interest. The test case is the preliminary design of an organic Rankine cycle turbogenerator to increase the overall energy efficiency of an offshore platform. For an increase in expander pressure ratio from 10 to 35, the results indicate up to 10% point reduction in expander performance. This corresponds to a relative reduction in net power output of 8.3% compared to the case when the turbine efficiency is assumed to be 80%. This work also demonstrates that this approach can support the plant designer in the selection of the optimal size of the organic Rankine cycle unit when multiple exhaust gas streams are available.

Keywords: organic Rankine cycle (ORC); turbine design; cycle optimization; turbine performance; surrogate model; axial turbine; mean line model

1. Introduction

Environmental concerns stress the need for reducing greenhouse gas emissions and pollutants. Organic Rankine cycle (ORC) power systems have proved to be a reliable, efficient and cost-competitive solution for heat-to-power conversion in the industrial and transport sector. Current research efforts aim at enlarging their application range by improving the performance of mini-ORC

systems (3–20 kW) for challenging low heat source temperatures (90–150 °C) [1]. Concurrently, ORC units are also a consolidated technology for medium-low temperatures (150–300 °C) and viable alternatives to steam Rankine cycle plants at high temperatures (300–500 °C) in niche sectors where the advantages of the ORC technology can be entirely exploited [2,3].

In the medium-low range of power, both the variety and the specific properties of the available working fluids make the expander the most expensive component [4] as well as the most challenging one to design. Several kinds of expanders are available for ORC applications, but in the medium-high range of power, radial or axial turbines are the preferred technologies [5]. The turbine is arguably the most critical component, owing to the small volumetric flow rates and the high expansion ratios [6]. The turbine performance tightly relates to the layout of the thermodynamic cycle, and its design is of paramount importance for the technical and economic optimization of the power module. Numerous studies on the maximization of the cycle performance are available in the literature, see, e.g., [4,5,7,8]. A detailed and thorough design of such power plants would require the simultaneous optimization of both the expander and cycle itself for the particular case study.

Few works, however, address the feasibility of the turbine design, and those which do, typically consider it *a posteriori* or by setting bounds on the cycle parameters. As an example, Kang [9] selected the evaporation pressure of a 200 kW ORC unit with R245fa as the working fluid, considering 4.11 as the maximum limit for the expansion ratio. Invernizzi *et al.* [10] employed the volumetric expansion ratio and the size parameter to identify a suitable working fluid for a bottoming mini-ORC unit. Astolfi *et al.* [11] performed a techno-economic optimization of a geothermal ORC power system, by estimating the number of turbine stages using information on the maximum volume flow ratio and the largest enthalpy drop. In another work, Astolfi and Macchi [12] addressed the problem by developing regression equations to compute efficiency from a set of optimized turbine designs.

Part A of this two-part paper has presented the structure and validation of the axial turbine simulation tool, TURAX, which provides the preliminary design of single-stage axial-flow turbines [13]. In addition, a sensitivity analysis has been performed in order to reduce the number of decision variables required for the turbine design optimization. The objective of the present part B of the paper is to quantify the impact of the simultaneous optimization of the expander and cycle design on the overall cycle performance. The relevance of this topic has been already addressed in some works, such as the study proposed by Uusitalo *et al.* [14]. The authors investigated the turbine design for low-power range ORC systems considering different organic fluids and stressed the relevance of coupling the turbine and the thermodynamic design processes.

To this end, a steady-state model of the thermodynamic cycle is coupled to the turbine simulation tool. This integration is performed by optimizing the expander geometry for different boundary conditions of the cycle, *i.e.*, mass flow rate and pressure ratio. Based on the optimization results, a surrogate model of the turbine is built to provide the maximum isentropic efficiency as a function of the boundary conditions. The adopted procedure allows for reducing the computational cost required by a combined optimization of expander and cycle. The case study is the preliminary design of an ORC unit used to increase the overall energy efficiency of an offshore platform by utilizing the waste heat from on-board gas turbine exhaust gases.

Compared to conventional thermodynamic cycle analyses, this approach gives a more realistic picture of the energy conversion efficiency of the system, when changing the key thermodynamic parameters of the cycle or scaling the dimension and power range of the plant. The results are compared with those obtained assuming a constant isentropic turbine efficiency, thus demonstrating the impact of a proper modeling of the turbine for this class of power systems.

The coupling of expander and cycle tools to estimate the design of an ORC system has been presented by Ventura and Rowlands [15] and Uusitalo *et al.* [14]. One difference compared with the present work is that a radial inflow turbine configuration was considered in both studies, whereas an axial turbine design is considered herein. Moreover, both of the cited works did not optimize the design of the machine: Ventura and Rowlands [15] obtained the expander performance from a

database, whereas Uusitalo *et al.* [14] set the turbine efficiency to 80%. On the contrary, in the present work, a simultaneous optimization of both cycle and expander designs is carried out. In conclusion, to the authors' best knowledge, this is the first time a mean-line validated axial turbine design tool is presented and coupled with an ORC cycle model for the simultaneous optimization of the expander and cycle design using advanced optimization algorithms.

The paper is structured as follows: Section 2 presents the case study of this work. Section 3 recalls the optimization of the turbine and discusses its integration in the cycle thermodynamic optimization through the mean-line turbine simulation tool. The results are then reported and discussed in Section 4. The conclusions are given in Section 5.

2. The Case Study

The power system installed on the Draugen oil and gas offshore platform is chosen as the case study. The platform is located 150 km from Kristiansund, in the Norwegian Sea. Three Siemens SGT-500 gas turbines [16] are installed on the platform. The electrical power demand on board is 19 MW. Two turbines are kept in operation at all times, each covering 50% of the load. The third is kept on stand-by, allowing for maintenance work. Despite the low energy conversion efficiency, this strategy ensures the necessary reserve power for peak loads and the safe operation of the engines.

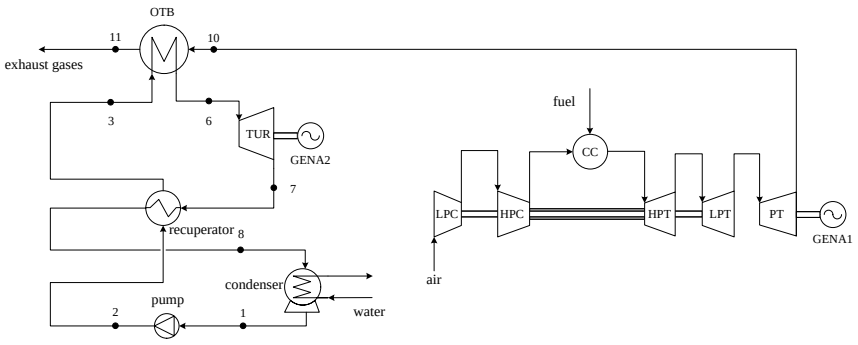

Figure 1. Simplified layout of the power system on the Draugen offshore oil and gas platform; the exhaust gases of one engine feed the organic Rankine cycle module. The two remaining gas turbines are not shown. Once-through boiler: OTB; low pressure compressor: LPC; high pressure compressor: HPC; low pressure turbine: LPT; high pressure turbine: HPT; power turbine: PT. Combustion chamber: CC; Organic Rankine cycle turbine: TUR.

The Siemens SGT-500 gas turbine takes with natural gas and generates an electric power output of 16.5 MW. The mass flow rate and the temperature of the exhaust gases discharged by the engine are equal to 91.5 $kg \cdot s^{-1}$ and 625 K [4], respectively. The twin-spool engine is equipped with two coaxial shafts: the first one couples the low pressure compressor (LPC) with the low pressure turbine (LPT), while the second one couples the high pressure compressor (HPC) with the high pressure turbine (HPT) [16]. The power turbine (PT) transfers mechanical power through a dedicated shaft to the electric generator (GEN). Recuperating the exhaust thermal power of the engines with an ORC unit will enhance their energy conversion efficiency. Figure 1 shows the layout of the power system, where one ORC unit is considered as the bottoming unit for one gas turbine. The relatively low temperature of the exhaust gases allows transferring the heat directly to the once-through boiler (OTB), avoiding an intermediate oil loop. After the expansion in the ORC turbine (TUR), the working fluid releases heat in the recuperator. In this way, the temperature of the organic compound at the OTB inlet may be increased by exploiting the residual energy of the exhausted vapor exiting the turbine. The ORC fluid is then condensed and compressed to the highest pressure level and preheated through the recuperator, thus closing the cycle. The selected organic compound is cyclopentane, since it leads to the simultaneous optimization of the net present value, plant efficiency and volume of the investigated ORC unit [4]. Moreover, this organic compound is already adopted for operating ORC systems in this range of temperatures [17].

3. Methods

3.1. Optimization Tools

ORC turbines entail small enthalpy drops and higher volume flow ratios per stage compared to gas and steam turbines. The main problem is thus to distribute the load between stator and rotor in the most effective way. As discussed by Macchi [6], it is necessary to find a compromise between a pure impulse stage and a conventional configuration with a degree of reaction set to 0.5. The former implies a high Mach number of the relative velocity at the rotor inlet, causing losses. Conversely, the latter demands prohibitive rotor blade height variations between inlet and outlet. A detailed analysis is, therefore, necessary to find the optimal solution.

For the purpose of this work, an in-house code for turbine preliminary design, called TURAX, was written in the Matlab language. The code has been extensively described in part A; here, the main features of the code are briefly summarized.

For a given set of design parameters and boundary conditions, *i.e.*, mass flow rate, inlet temperature, rotational speed and total pressure ratio, the simulation tool produces a preliminary design of a single-stage machine (see Figure 2 for blade nomenclature) and an estimation of the total-to-total isentropic efficiency. Similar to other preliminary design codes available in the literature, such as zTurbo [18], TURAX is based on one-dimensional approximation supported by proper correlations for the estimation of the losses and flow angles [19,20].

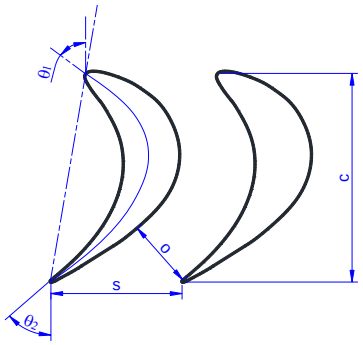

Figure 2. Main geometric blade parameters with relative nomenclature.

The code is integrated with the optimization toolbox available in the Matlab framework [21] to obtain the turbine layout which maximizes the total-to-total isentropic efficiency. In order to find the optimal solution, a particle swarm optimization (PSO) [22] is first performed for a given number of generations. Afterwards, the Audet–Dennis generalized pattern search (GPS) algorithm is executed [23]. By searching in the vicinity of each optimizing parameter, this method allows for optimizing further the optimal solution given by the PSO.

Compared to gradient-based methods, evolutionary algorithms are less prone to end the search in local minima of the problem and in principle allow converging towards global optima. This typically comes at the expense of an increased computational effort, due to the large number of the objective function evaluations [24]. Computational fluid dynamics tools tackle this issue by resorting to self-learning metamodels of the response surface [25]. However, in the present case, the computational burden of a single evaluation is comparatively small, and it does not justify the use of metamodels.

Compared to the evolutionary algorithm reported in Mahalakshmi *et al.* [26], the combination of particle swarm and pattern search optimization could reduce the computational time, providing a more straightforward way to detect the optimal solution [27]. This is due to the possibility of introducing inertia weight parameters in PSO, which allows for free-tuning the current search area

of solutions [28]. Indeed, providing a proper selection of the inertia weight allows for obtaining a suitable balance between global and local exploration abilities; hence, the method is likely to require fewer iterations on average to find the optimum. The particle swarm was run assigning a population size of 1000 and a maximum iteration number of 20. These numerical values are selected to ensure the repeatability of the solution when different simulations are performed.

The vector of optimizing variables at hand reads:

$$\overline{X} = \left[\psi, o_{\mathrm{min}}, o_{\mathrm{r}}, c_{\mathrm{n}}, c_{\mathrm{r}}, \left(o/s\right)_{\mathrm{n}}, \left(o/s\right)_{\mathrm{r}}, C_{\mathrm{a1}}, \phi_{\mathrm{r}}, N\right], \quad (1)$$

where ψ is the stage loading coefficient, C_{a1} is the stage inlet axial velocity, ϕ_{r} is the rotor flow coefficient and N is the rotational speed of the machine, if considered among the optimization variables. The geometric variables o and c are the blade throat opening and the axial chord (see Figure 2). The possible choice of seeking a turbine geometry optimized for a certain rotational speed implies the insertion of a gearbox in order to match the frequency of the machine with that of the generator. The initialization of the optimizer requires setting the upper and lower bounds, limiting the optimization variables.

Additional constraints on the geometry and thermodynamic variables are necessary to provide acceptable solutions from physical and technological perspectives. These conditions, established by Macchi and Perdichizzi [29], Vavra [30] and Saravanamuttoo *et al.* [31], are accordingly implemented as non-linear constraints. The first part of Table 1 lists the upper and lower bounds imposed on the dependent and independent variables. As a consequence of these bounds, solutions featuring highly supersonic flows at the stator-exit are accepted; conversely, configurations entailing supersonic relative flow at rotor inlet and outlet are discarded. This choice is made in order to avoid unique incidence effects that dramatically complicate the blade design and the power control capability. Moreover, a high supersonic flow at the rotor-exit would require converging-diverging rotor blades.

Table 1. Lower and upper bounds for the decision variables, constraints and fixed parameters.

Decision Variable	Lower Bound	Upper Bound
Stage loading coefficient ψ (-)	2	6
Nozzle minimum opening o_{min} (mm)	2	100
Rotor opening o_{r} (mm)	2	100
Nozzle axial chord c_{n} (mm)	10	100
Rotor axial chord c_{r} (mm)	10	100
Nozzle outlet opening-to-pitch ratio $(o/s)_{\mathrm{n}}$ (-)	0.225	0.7
Rotor outlet opening-to-pitch ratio $(o/s)_{\mathrm{r}}$ (-)	0.225	0.7
Stage inlet axial velocity C_{a1} ($\mathrm{m \cdot s^{-1}}$)	0	100
Rotor flow coefficient ϕ_{r} (-)	0	1
Rotational speed (if optimized) N (rpm)	2000	100,000
Additional constraints		
Relative Mach number at the rotor inlet (-)	0	0.8
Relative Mach number at the rotor outlet (-)	0	1.4
Number of nozzle blades (-)	10	130
Number of rotor blades (-)	10	130
Flare angles (°)	-25	25
Blade height to mean diameter ratio h/D_{m} (-)	0.001	0.25
Axial chord to mean diameter ratio c/D_{m} (-)	0.001	0.2
Reynolds number (-)	10^4	$+\infty$
Fixed parameters		**Value**
Rotor inlet height/nozzle outlet height (-)		1
Mach number for the transition to converging-diverging nozzle (-)		1.4
Nozzle trailing edge/pitch (-)		0.05
Rotor trailing edge/pitch (-)		0.05
Radius of blade rear suction side curvature (m)		10^6
Nozzle-rotor axial clearance (m)		$c_{\mathrm{n}}/2$
Blade absolute surface roughness (m)		2×10^{-6}
Minimum blade trailing edge thickness (m)		2×10^{-4}
Minimum rotor tip clearance (m)		$\max\{D_{\mathrm{m}}/2000; 2 \times 10^{-4}\}$

Finally, some fixed parameters need to be set when the optimization routine starts. These latter ones are reported in the second part of Table 1.

Through this procedure, turbine efficiency is optimized for several sets of boundary conditions. This allows the construction of a line of optimal configurations for the particular application. Figure 3 shows how the surrogate models are inserted in the plant model, while Figure 4 summarizes the optimization procedure and the creation of surrogate models.

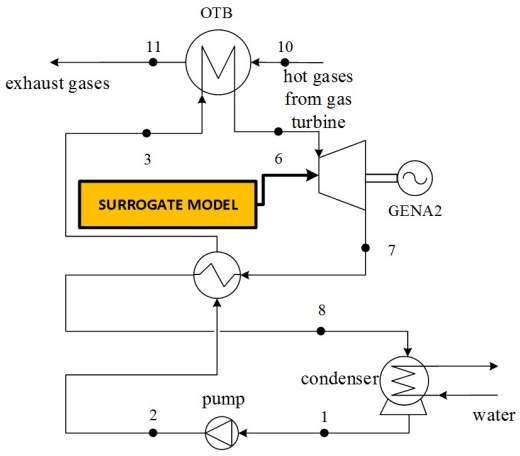

Figure 3. Organic Rankine cycle (ORC) plant layout showing the coupling with turbine surrogate models.

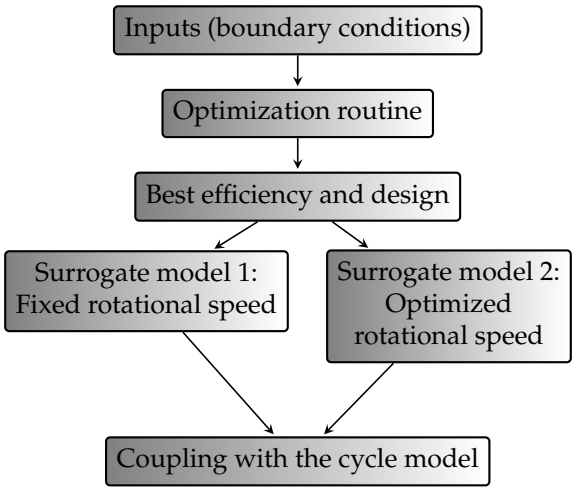

Figure 4. Diagram illustrating the expander optimization procedure and integration with the cycle model.

3.2. Thermodynamic Cycle Calculation

The computation of the thermodynamic states is accomplished by applying the energy and mass balance equations to each plant constituent. This procedure yields the computation of the thermodynamic states at the inlet and outlet of each system component. Figure 5 illustrates the $T - s$ diagram for an ORC module with a turbine inlet pressure of 3 MPa. The nodes where the working fluid is in saturated conditions, *i.e.*, 4, 5 and 9 in Figure 5, are not reported in the plant layout (Figure 1). The evaporation and condensation start inside the boiler and the condenser, respectively. A constant pressure specific heat capacity of $1100\,\mathrm{J}\cdot\mathrm{kg}^{-1}\cdot\mathrm{K}^{-1}$ is used for the energy balance calculations involving the exhaust gases. Since supercritical configurations would imply

values of pressure ratio that are too high for a single-stage turbine, this work considers only subcritical cycle configurations.

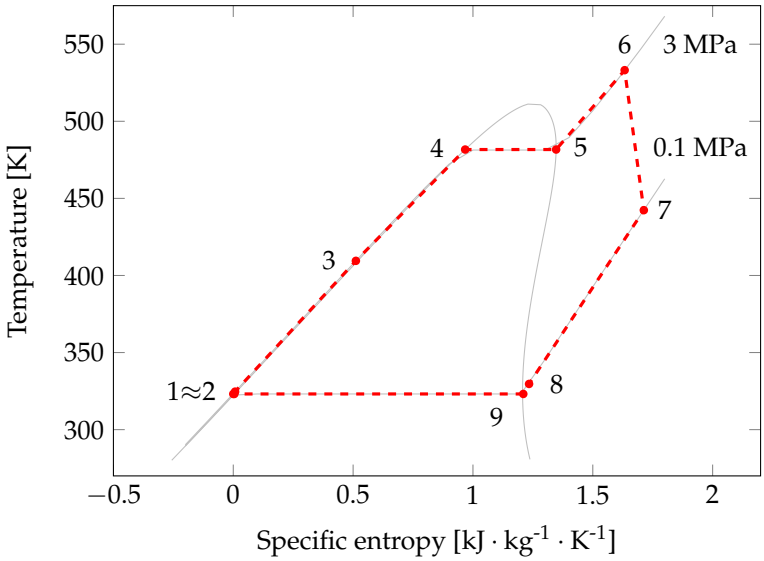

Figure 5. Saturation curve of cyclopentane in a $T - s$ diagram, showing the thermodynamic cycle state points of the organic Rankine cycle system.

The condensing pressure is equal to 10^5 Pa to prevent air leakages into the engine. The pinch-point temperature differences of the boiler and internal recuperator are fixed to 10 and 15 K, respectively. The pump isentropic efficiency and the electrical efficiency of the generator are equal to 0.8 and 0.98 [4]. Additional assumptions are the following: no pressure loss in piping or heat transfer equipment, adiabatic system, steady-state condition and homogeneous flow in terms of thermodynamic properties. Note that the turbine inlet temperature is kept at 513.15 K to ensure the chemical stability of the working fluid. The reader is referred to Pasetti *et al.* [32] for an in-depth analysis of the cyclopentane decomposition at high temperatures. According to the values reported by Walsh and Fletcher [33], a gearbox efficiency of 0.98 is used when the rotational speed is included in the turbine optimization.

4. Results and Discussion

Figures 6 and 7 show the results for the turbine optimization at constant rotational speed (3000 rpm) and for the optimized rotational speed. The plots relate the total-to-total isentropic efficiency to the mass flow rate of the working fluid and the pressure ratio $\pi_e = p_{06}/p_{07}$. Each point in the figures represents a different optimal geometry obtained with a dedicated optimization. Figure 8 shows an example of optimal geometry with relative velocity triangles. It is interesting to note that, in the present generalized approach, the not-null tangential velocity at the stage-exit results from a systematic optimization applied to minimize the aerodynamic losses. Figure 9a reports a breakdown of turbine losses for the optimal geometries obtained for $\pi = 20$ assuming constant rotational speed; Figure 9b reports the same trend for the geometries obtained optimizing also the rotational speed. In Figure 6, the efficiency curves initially increase as a function of the mass flow rate and subsequently flatten out. Figure 9a shows that secondary and tip clearance losses are mainly responsible for this behavior; the same chart also shows that for the same pressure ratio, as the mass flow rate increases, secondary and tip clearance losses are reduced. Indeed, for higher mass flow rates, the turbine size increases proportionally, resulting in wider blade channels and reduced relative influence of secondary and tip clearance losses. The results are in line with the trends reported by Macchi and Perdichizzi [29] for complex and monoatomic gases.

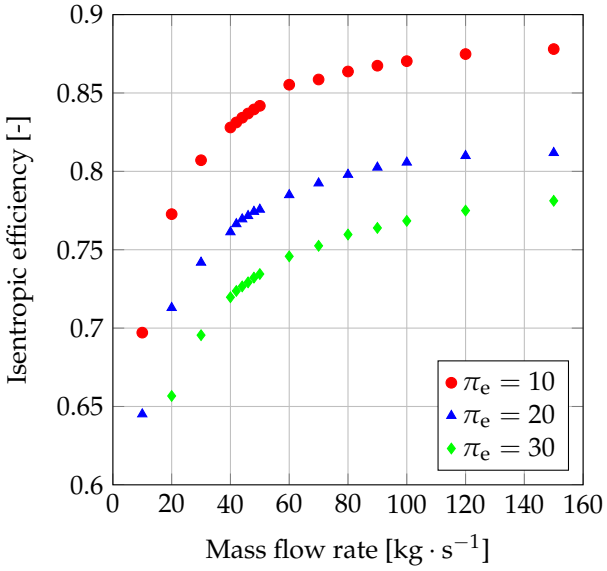

Figure 6. Surrogate turbine model at fixed rotational speed, relating total-to-total isentropic efficiency to the mass flow rate and pressure ratio across the turbine.

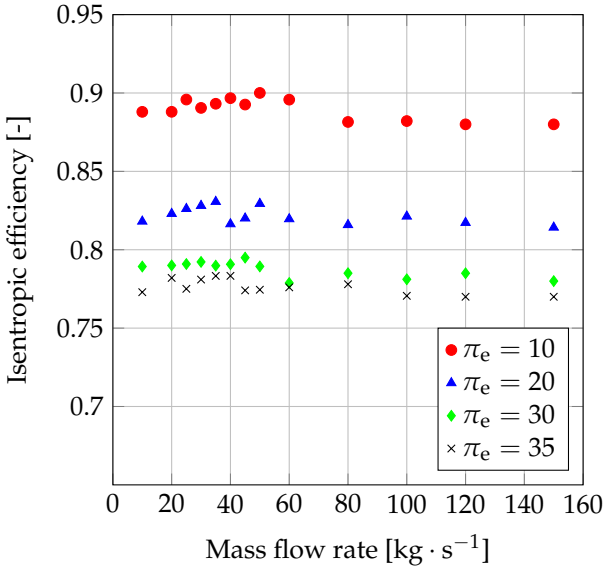

Figure 7. Surrogate turbine model at the optimal rotational speed, relating total-to-total isentropic efficiency to the mass flow rate and pressure ratio across the turbine.

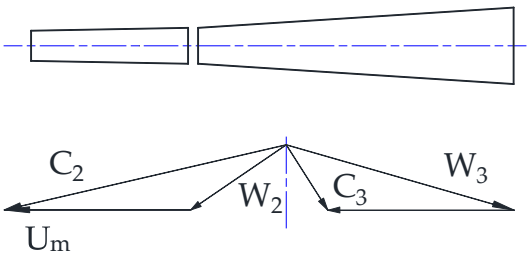

Figure 8. The turbine section channel and relative velocity triangles at $\pi_e = 10$ and $10\,\mathrm{kg \cdot s^{-1}}$. The degree of reaction is 0.2 and the rotational speed is fixed to 3000 rpm.

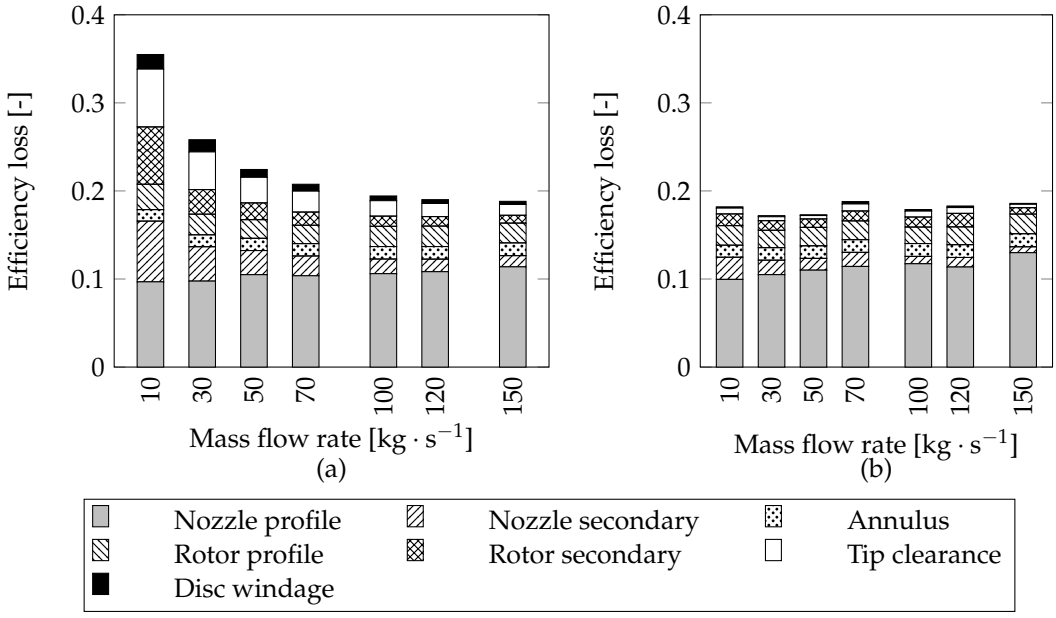

Figure 9. Losses breakdown for the optimal geometries obtained considering: (**a**) constant rotational speed and (**b**) optimized rotational speed. Turbine losses *versus* mass flow rate for $\pi = 20$. The efficiency loss is defined as the complementary fraction for efficiency to reach unity.

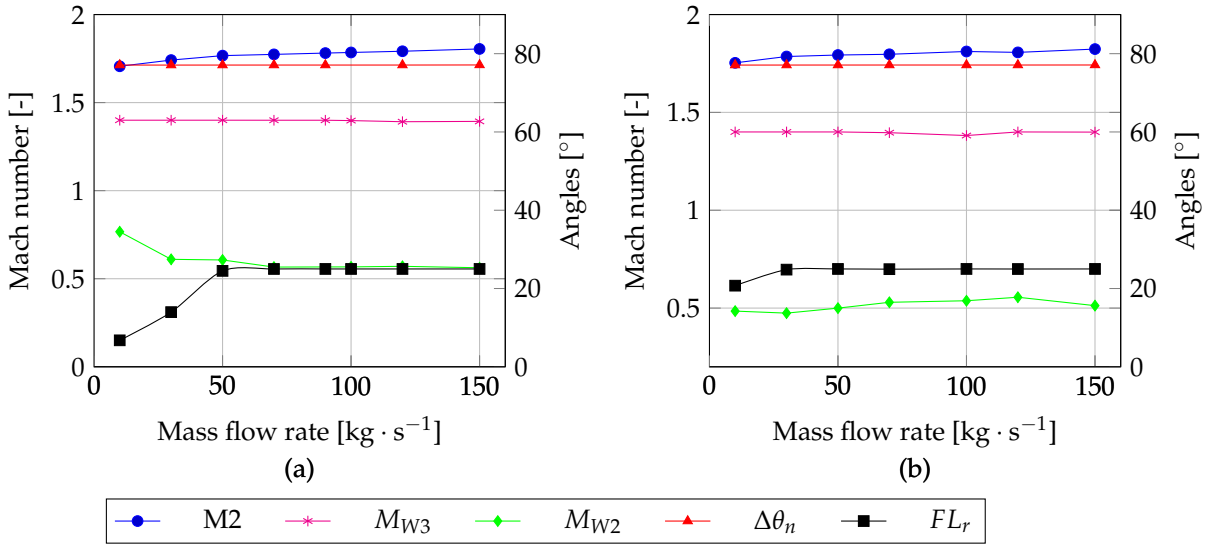

Figure 10. Angles and Mach numbers for the optimal geometric configurations for $\pi = 20$ as a function of mass flow rate: (**a**) constant rotational speed and (**b**) optimized rotational speed.

Figures 10 and 11 report the trend of some turbine parameters obtained for the optimized geometries as a function of mass flow rate and $\pi = 20$. Figure 10a shows that the rotor flare angle reaches the maximum allowed value of 25° at around 50 kg · s^{-1}; when the rotational speed is also optimized, this parameter almost always reaches the upper bound (see Figure 10b). Similarly, the blade deflection in the nozzle $\Delta\theta_n$ always reaches the upper limit. The losses breakdown of Figure 9a,b show that the nozzle has to bear most of the expansion, even though both the optimization processes produced optimal geometries where the nozzle profile losses are kept averagely at a constant value. This happens despite the high and slightly increasing value of Mach number M_2, as reported in Figure 10a,b. The same charts show also how the rotor inlet relative Mach number M_{W2} is always held considerably below the upper constraint of 0.8 listed in Table 1. Finally, Figure 11a,b

show that at higher mass flow rate, both the nozzle and rotor aspect ratios increase, yielding higher blade channels and lower nozzle secondary losses.

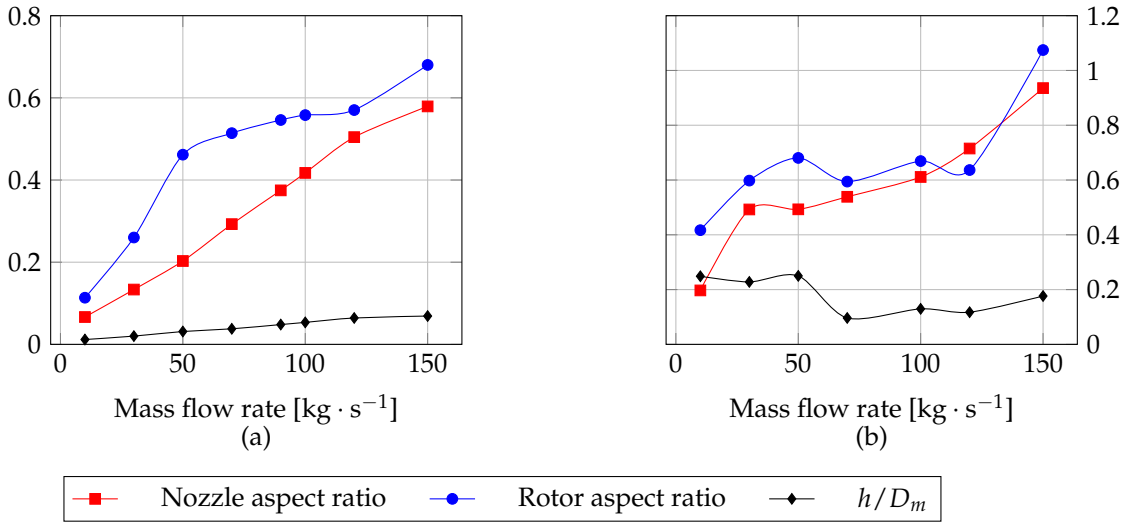

Figure 11. Additional turbine adimensional parameters for the optimal geometric configurations for $\pi = 20$ as a function of mass flow rate: (**a**) constant rotational speed and (**b**) optimized rotational speed.

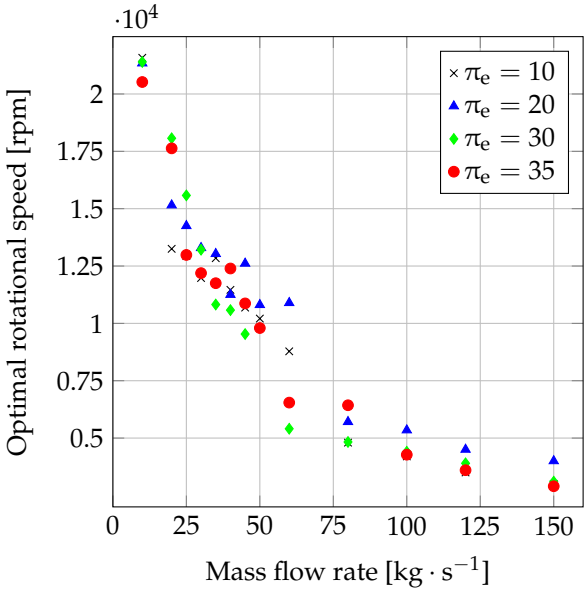

Figure 12. Optimal rotational speed *versus* mass flow rate at different turbine pressure ratios.

Removing the constraint on the rotational speed is beneficial for the expander design, especially at low mass flow rate. Figure 12 reports the optimal values obtained for the rotational speed as a function of mass flow rate and clearly indicates the monotone increasing trend of optimal angular speed as the mass flow rate reduces. Figure 13 shows a breakdown of losses as a function of the pressure ratio for the geometries obtained optimizing the rotational speed for 50 kg · s^{-1}. Figures 14 and 15 report the trends of some turbine parameters obtained for these optimized configurations. The new decision variable allows for obtaining geometric layouts that constantly keep secondary and tip clearance loss coefficients at a minimum. According to Figure 7, the highest gain in the turbine efficiency occurs indeed at mass flow rates lower than 80 kg · s^{-1}. Conversely, operating at constant

rotational speed leads to an increment of the turbine losses for decreasing mass flow rates. In this case, as confirmed by Figures 14 and 15, the turbine blade aspect ratio decreases, and consequently the secondary losses increase.

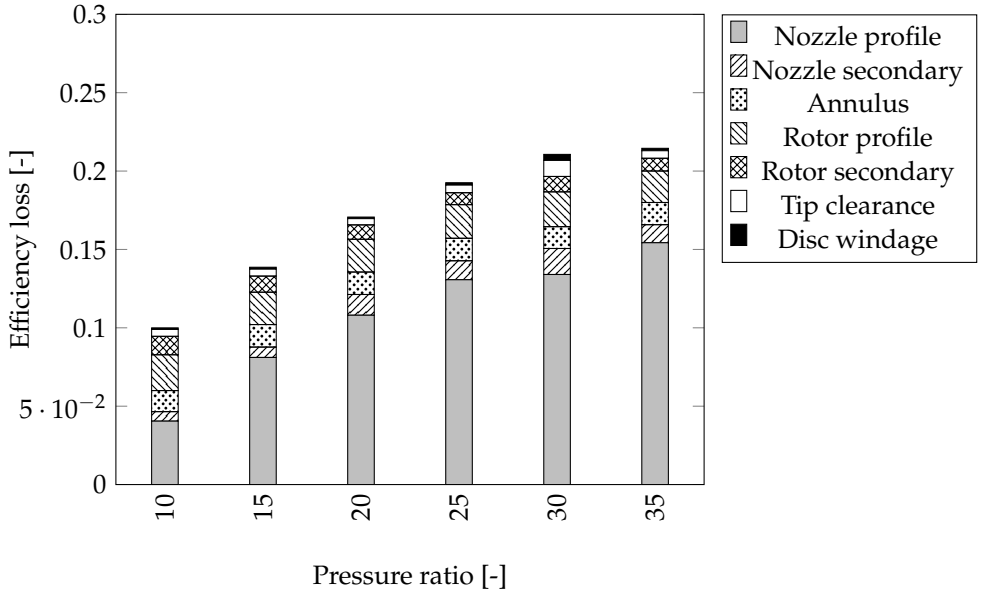

Figure 13. Losses breakdown for the optimal geometries obtained considering optimized rotational speed. Turbine losses *versus* pressure ratio for $\dot{m} = 50\ \mathrm{kg} \cdot \mathrm{s}^{-1}$.

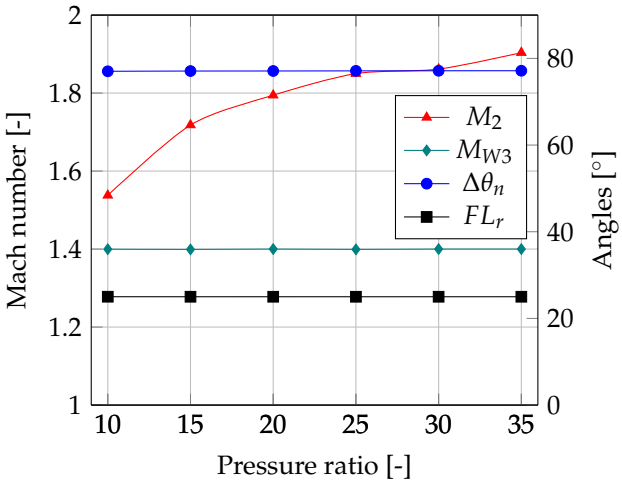

Figure 14. Turbine and flow parameters for the optimal geometric configurations with optimized rotational speed. Pressure ratio *versus* nozzle and rotor Mach numbers on the left axis; nozzle blade deflection and rotor flare angle on the right axis.

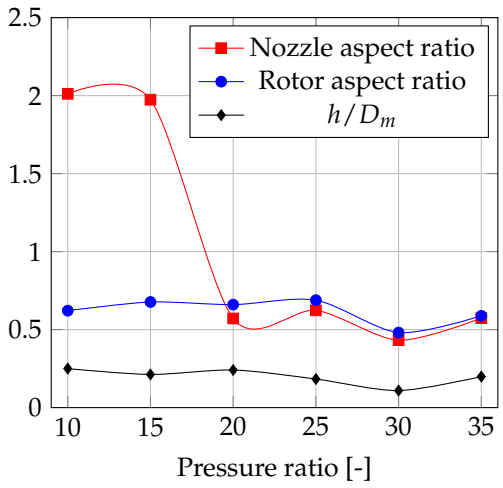

Figure 15. Turbine and flow parameters obtained for the optimal geometric configurations with optimized rotational speed. Pressure ratio *versus* nozzle and rotor aspect ratio and rotor outlet blade height to average diameter.

As shown in Figure 7, when the turbine rotational speed is optimized, the mass flow rate has a reduced influence on the turbine efficiency. On the other hand, the pressure ratio still plays a major role. Figure 13 shows a marked increment in nozzle profile losses for increasing values of the pressure ratio. This can be explained by the increasing values of nozzle velocity components; indeed, increasing the pressure ratio makes the nozzle bear an increasingly more consistent part of the expansion. This is reflected by the trend of nozzle Mach number M_2 in Figure 14. The same chart also shows that the rotor relative Mach number M_{W3}, the blade deflection in nozzle $\Delta\theta_n$ and the rotor flare angle FL_r always reach the upper bounds of Table 1.

Finally, the possibility of also optimizing the rotational speed enables higher expansion ratios with just a single stage: raising the pressure ratio entails higher Mach numbers, velocities and flare angles which, for a case with fixed rotational speed, would make the final geometry violate the superimposed constraints. The higher degree of freedom introduced with the optimization of rotational speed enables avoiding the violation of the constraints. Moreover, higher pressure ratios for the chosen turbine inlet temperature bring the inlet working point closer to the critical/two-phases region.

Figure 16a compares the ORC net power output at different constant isentropic efficiencies with the one calculated using the turbine surrogate models, labeled as TURAX and TURAX-N, respectively, for fixed and optimized rotational speed. Given the assumptions reported in the previous section, π_e is the primary variable affecting the power output, since in this case the mass flow rate varies between 45 and 50 $kg \cdot s^{-1}$ for the reported range of π_e. The constant isentropic efficiency curves differ significantly compared to the trends observed with the surrogate models. This is due to the progressive decrement of the expander performance at increasing pressure ratios, as visible in Figure 16b. The computed isentropic efficiency decreases from 0.82 to 0.74 for the case with fixed rotational speed. The curve intersects the horizontal lines which refer to the cases with constant efficiency. Accounting for the variability of the expander performance yields a maximum difference in power output of 500 kW, compared to the results obtained assuming a fixed turbine efficiency of 80% at $\pi_e = 30$. This corresponds to a relative power decrement of 8.3%.

Figure 16b demonstrates that the optimization of the rotational speed increases on average the expander efficiency by 5%-points. The power curve is labeled as TURAX-N in Figure 16a,b. For $\pi_e = 30$, the improvement in power output compared to the case with constant rotational speed is around 250 kW, corresponding to a relative increment of 4.5%. This gain relates to the fact that the ORC unit operates in the range of mass flow rates where optimizing the rotational speed is highly beneficial for the expander efficiency (see Figures 6 and 7). However, a turbine with optimized

rotational speed allows for reaching a higher pressure ratio with a further increment of power. The highest power output occurs at the maximum available pressure ratio with just one stage, *i.e.*, 35 for a turbine with optimized rotational speed. Here, the volumetric flow ratio reaches 43.5, a value close to 50, the upper limit suggested by Macchi [6]. Further increments in the power output could be achieved by increasing the number of stages. On the other hand, a larger number of stages implies higher investment costs. Moreover, the power curve in Figure 16b, obtained using the surrogate model, shows a progressively flattening trend for high values of pressure ratio if a single-stage turbine is adopted. It is expected that the small power increments do not justify the technological (and economic) effort to operate at higher pressures. A complete techno-economic optimization must be carried out, in order to draw quantitative conclusions. However, such analysis is beyond the scope of the current paper.

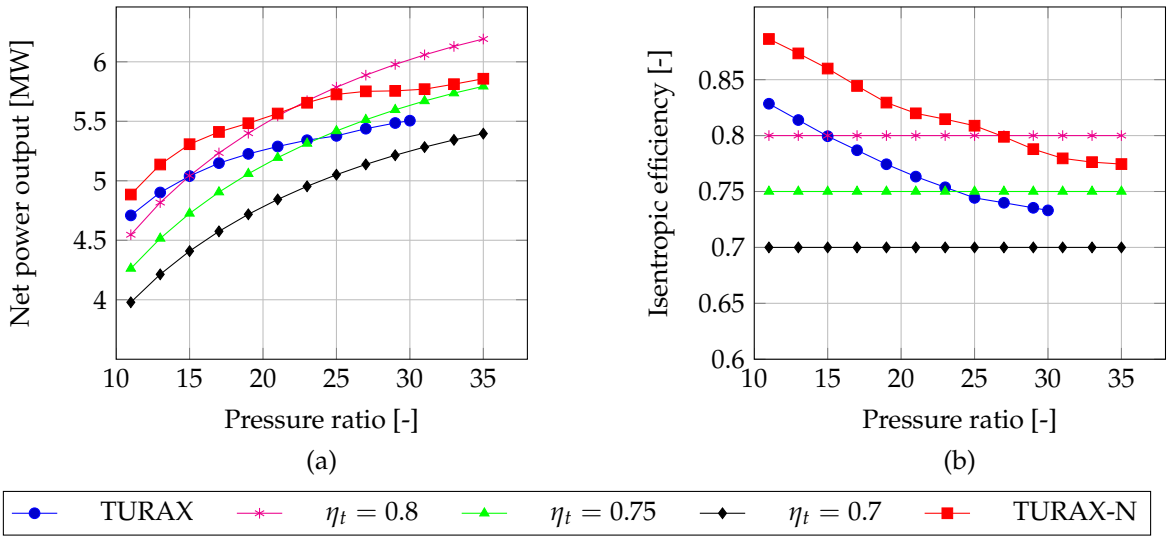

Figure 16. (**a**) net power output *versus* pressure ratio and (**b**) total-to-total turbine isentropic efficiency *versus* pressure ratio for an ORC unit utilizing exhaust gas heat from one gas turbine.

Figure 6 shows that the total-to-total isentropic efficiency of the turbine with constant rotational speed reaches the maximum after 120 $kg \cdot s^{-1}$. This value is around three times the mass flow rate of the ORC unit fed by the exhaust gases of one gas turbine. Given that, on the Draugen platform, two engines typically operate at the same time, the opportunity arises of harvesting the heat from both energy sources with one ORC unit. This investigation assumes perfect mixing of the two exhaust gases and that the gas turbines are sharing the load equally. As reported in Figure 17a, the trend of power *versus* pressure ratio is similar to that presented in the previous test case. However, the power output obtained with the surrogate model is proportionally larger, since the values of turbine efficiency are around eight percentage points higher. The integration of the ORC unit with one engine produces a net power of 5.5 MW. Conversely, the use of the exhaust heat of two gas turbines gives a total output of 11.5 MW. Therefore, the latter plant configuration offers a relative power increment of 4.5%, compared to the implementation of two separate ORC turbogenerators. As shown in Figure 17b, the use of one ORC unit for two engines significantly reduces the benefit of optimizing the rotational speed of the turbine. The increment in efficiency is much smaller compared to the case of two separate ORC power systems. Moreover, Figure 17a shows that the mechanical losses of the gearbox almost overshadow the gain in turbine efficiency.

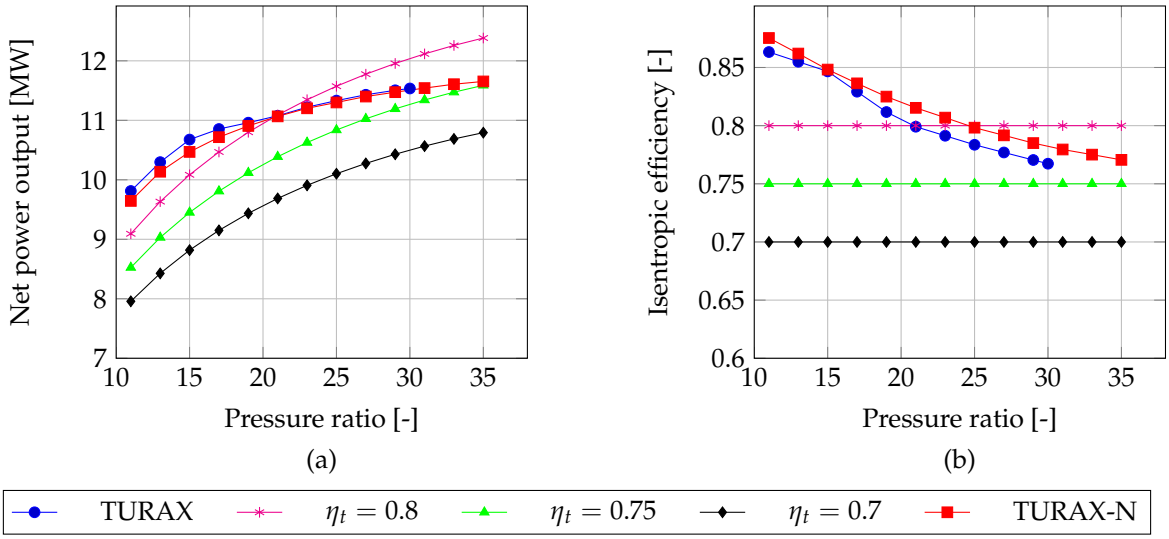

Figure 17. Multiple exhaust gas configuration. (**a**) net power output *versus* pressure ratio and (**b**) total-to-total turbine isentropic efficiency *versus* pressure ratio.

5. Conclusions

This two-part paper documented the development of a simulation tool for the preliminary design of axial turbines and the integration of this tool within the optimization of a complete power plant. In the present paper, the axial turbine simulation tool was combined with the thermodynamic model of the ORC process. The coupling was enabled through a surrogate model, which relates the optimal turbine efficiency to the actual boundary conditions given by the thermodynamic cycle. The method was applied to design an ORC power system for offshore applications.

The results obtained by computing the expander performance with the surrogate model were compared with those assuming constant turbine isentropic efficiency. The power curves exhibit different trends with a maximum relative discrepancy of 8.3% in power output. The results indicate that the net power output of the ORC unit increases for an increasing pressure ratio. On the other hand, the performance of the turbine decreases as the pressure ratio increases. Taking into account the variation of the turbine efficiency rather than assuming a constant value results in reduced benefits of high cycle pressures. For the case of exhaust heat recovery from a single gas turbine, the optimization of the rotational speed of the machine improves expander performance by five percentage points, with a corresponding relative increment in net power of 5% for the ORC unit. For the case where a single ORC turbogenerator utilizes the exhaust heat from two gas turbines, a 4.5% improvement in power output is achieved compared to an implementation where the two gas turbines are fitted with individual ORC units. This latter configuration makes the optimization of the rotational speed not attractive, since the increased mechanical losses almost overshadow the higher turbine isentropic efficiency.

Acknowledgments: The research work was conducted within the frame of the THERMCYC project ("Advanced thermodynamic cycles utilizing low-temperature heat sources"; see http://www.thermcyc.mek.dtu.dk/) funded by InnovationsFonden, The Danish Council for Strategic Research in Sustainable Energy and Environment.

Author Contributions: Angelo La Seta is the main author of this work. Andrea Meroni contributed to the development of the turbine model code. Jesper Graa Andreasen and Leonardo Pierobon structured the first version of the code, subsequently improved by Angelo La Seta and Andrea Meroni, and helped during the overall optimization setup process and writing. Review and guidance of the work was provided by Giacomo Persico and Fredrik Haglind.

Conflicts of Interest: The authors declare no conflict of interest.

Nomenclature

C Absolute fluid velocity ($m \cdot s^{-1}$)
D Turbine diameter (m)
FL Flare angle (°)
M Mach number (-)
N Rotational speed (rpm)
U Peripheral velocity ($m \cdot s^{-1}$)
W Relative fluid velocity ($m \cdot s^{-1}$)
$\overline{X}$ Array of the optimizing variables
c Axial chord (m)
h Blade height (m)
o Blade opening (m)
p Pressure (Pa)
s Blade pitch (m)

Abbreviations and Acronyms

CC Combustion chamber
GEN Electric generator
GPS Global pattern search
HPC High pressure compressor
HPT High pressure turbine
LPC Low pressure compressor
LPT Low pressure turbine
ORC Organic Rankine cycle
OTB Once-through boiler
PSO Particle swarm optimization
PT Power turbine
TUR Organic Rankine cycle turbine

Greek Letters

$\Delta\theta$ Blade deflection (°)
η_t Turbine isentropic efficiency (-)
π_e Pressure ratio (-)
ψ Stage loading coefficient (-)
θ Blade angle (°)

Subscripts

1 Nozzle inlet
2 Rotor inlet
3 Rotor outlet
a Axial component
m Referred to the average diameter
min Minimum opening
n Nozzle
r Rotor
W Relative velocity

References

1. Colonna, P.; Casati, E.; Trapp, C.; Mathijssen, T.; Larjola, J.; Turunen-Saaresti, T.; Uusitalo, A. Organic Rankine Cycle Power Systems: From the Concept to Current Technology, Applications, and an Outlook to the Future. *J. Eng. Gas Turbines Power* **2015**, *137*, 1–19.

2. Lang, W.; Colonna, P.; Almbauer, R. Assessment of waste heat recovery from a heavy-duty truck engine by means of an ORC turbogenerator. *J. Eng. Gas Turbines Power* **2013**, *135*, 1–10.
3. Casati, E.; Galli, A.; Colonna, P. Thermal energy storage for solar-powered organic Rankine cycle engines. *Sol. Energy* **2013**, *96*, 205–219.
4. Pierobon, L.; Nguyen, T.V.; Larsen, U.; Haglind, F.; Elmegaard, B. Multi-objective optimization of organic Rankine cycles for waste heat recovery: Application in an offshore platform. *Energy* **2013**, *58*, 538–549.
5. Quoilin, S.; Orosz, M.; Hemond, H.; Lemort, V. Performance and design optimization of a low-cost solar organic Rankine cycle for remote power generation. *Sol. Energy* **2011**, *85*, 955–966.
6. Macchi, E. Design criteria for turbines operating with fluids having a low speed of sound. *Von Karman Inst. Fluid Dyn.* **1977**, *2*, 1–64.
7. Larsen, U.; Pierobon, L.; Haglind, F.; Gabrielii, C. Design and optimisation of organic Rankine cycles for waste heat recovery in marine applications using the principles of natural selection. *Energy* **2013**, *55*, 803–812.
8. Andreasen, J.G.; Larsen, U.; Knudsen, T.; Pierobon, L.; Haglind, F. Selection and optimization of pure and mixed working fluids for low grade heat utilization using organic Rankine cycles. *Energy* **2014**, *73*, 204–213.
9. Kang, S.H. Design and experimental study of ORC (organic Rankine cycle) and radial turbine using R245fa working fluid. *Energy* **2012**, *41*, 514–524.
10. Invernizzi, C.; Iora, P.; Silva, P. Bottoming micro-Rankine cycles for micro-gas turbines. *Appl. Therm. Eng.* **2007**, *27*, 100–110.
11. Astolfi, M.; Romano, M.C.; Bombarda, P.; Macchi, E. Binary ORC (Organic Rankine Cycles) power plants for the exploitation of medium low temperature geothermal sources - Part B: Techno-economic optimization. *Energy* **2014**, *66*, 435–446.
12. Astolfi, M.; Macchi, E. Efficiency correlations for axial flow turbines working with non-conventional fluids. In Proceedings of the 3rd International Seminar on ORC Power Systems, Brussels, Belgium, 12–14 October 2015; pp. 1–12.
13. Meroni, A.; La Seta, A.; Andreasen, J.G.; Pierobon, L.; Persico, G.; Haglind, F. Combined Turbine and Cycle Optimization for Organic Rankine Cycle Power Systems-Part A: Turbine Model. *Energies* **2016**, *9*, doi:10.3390/en9050313.
14. Uusitalo, A.; Turunen-Saaresti, T.; Gronman, A.; Honkatukia, J.; Backman, J. Combined Thermodynamic and Turbine Design Analysis of Small Capacity Waste Heat Recovery ORC. In Proceedings of the 3rd International Seminar on ORC Power Systems, Brussels, Belgium, 12–14 October 2015; pp. 1–10.
15. Ventura, C.A.d.M.; Rowlands, A.S. Design and performance estimation of radial inflow turbines coupled with a thermodynamic cycle analysis procedure. In Proceedings of the 2nd International Seminar on ORC Power Systems, Rotterdam, The Netherlands, 7–8 October 2013; pp. 1–5.
16. Siemens. Gas Turbine SGT-500. Available online: http://www.energy.siemens.com/nl/en/fossil-power-generation/gas-turbines/sgt-500.htm#content=Description (accessed on 16 May 2016).
17. Del Turco, P.; Asti, A.; Del Greco, A.; Bacci, A.; Landi, G.; Seghi, G. The ORegen waste heat recovery cycle: Reducing the CO_2 footprint by means of overall cycle efficiency improvement. In Proceedings of the ASME Turbo Expo 2011, Vancouver, BC, Canada, 6–10 June 2011; pp. 547–556.
18. Pini, M.; Persico, G.; Casati, E.; Dossena, V. Preliminary design of a Centrifugal Turbine for Organic Rankine Cycles applications. *J. Eng. Gas Turbines Power* **2013**, *135*, 1–9.
19. Ainley, D.; Mathieson, G. *An examination of the flow and pressure losses in blade rows of axial-flow turbines*; Technical Report; Ministry of Supply-Aeronautical Research Council: London, UK, 1951.
20. Craig, H.; Cox, H. Performance estimation of axial flow turbines. *Proc. Inst. Mech. Eng.* **1970**, *185*, 407–424.
21. The MathWorks, Inc. *Optimization Toolbox ^{TM} User's Guide*; The MathWorks, Inc.: Natick, MA, USA, 2014.
22. Eberhart, R.C.; Shi, Y. Particle swarm optimization: developments, applications and resources. In Proceedings of the 2001 Congress on Evolutionary Computation, Seoul, Korea, 27–30 May 2001; Volume 1, pp. 81–86.
23. Audet, C.; Dennis, J.E. Analysis of generalized pattern searches. *SIAM J. Opt.* **2003**, *13*, 889–903.
24. Deb, K. *Multi-Objective Optimization Using Evolutionary Algorithms*; John Wiley & Sons, Inc.: West Sussex, UK, 2001; pp. 13–46.
25. Pasquale, D.; Persico, G.; Rebay, S. Optimization of Turbomachinery Flow Surfaces Applying a CFD-based Throughflow Method. *J. Turbomach.* **2013**, *136*, 1–11.

26. Mahalakshmi, M.; Kalaivani, P.; Nesamalar, E. A Review on Genetic Algorithm and its Applications. *Int. J. Comput. Algorithm* **2013**, *2*, 415–423.
27. Eberhart, R.C.; Shi, Y.; Porto, V.W.; Saravanan, N.; Waagen, D.; Eiben, A.E. Comparison between genetic algorithms and particle swarm optimization. In *Evolutionary Programming VII*; Springer: Berlin/Heidelberg, Germany, 1998; pp. 611–616.
28. Shi, Y.; Eberhart, R.C. A modified particle swarm optimizer. In Proceedings of the 1998 IEEE International Conference on Evolutionary Computation, Anchorage, AK, USA, 4–9 May 1998; pp. 69–73.
29. Macchi, E.; Perdichizzi, A. Efficiency prediction for axial-flow turbines operating with nonconventional fluids. *J. Eng. Gas Turbine Power* **1981**, *103*, 718–724.
30. Vavra, M.H. Axial Flow Turbines. *Von Karman Inst. Fluid Dyn.* **1969**, *15*, 1–117.
31. Saravanamuttoo, H.I.H.; Rogers, G.F.C.; Cohen, H. *Gas Turbine Theory*; Pearson Education: Upper Saddle River, NJ, USA, 2001.
32. Pasetti, M.; Invernizzi, C.M.; Iora, P. Thermal stability of working fluids for organic Rankine cycles: An improved survey method and experimental results for cyclopentane, isopentane and n-butane. *Appl. Therm. Eng.* **2014**, *73*, 762–772.
33. Walsh, P.; Fletcher, P. *Gas Turbine Performance*; Blackwell Science: Oxford, UK, 1998; pp. 1–628.